SCIENTIFIC REPORTS

OPEN

SUBJECT AREAS:
KINETICS
TRANSLATION

Received
22 August 2014

Accepted
5 December 2014

Published
8 January 2015

Correspondence and requests for materials should be addressed to H.J.W. (hj.wieden@uleth.ca)

* Current address: Department of Physical Biochemistry, Max-Planck Institute for Biophysical Chemistry, Göttingen, Germany.

A conserved P-loop anchor limits the structural dynamics that mediate nucleotide dissociation in EF-Tu

Evan Mercier*, Dylan Girodat & Hans-Joachim Wieden

Alberta RNA Research and Training Institute, Department of Chemistry and Biochemistry, University of Lethbridge, Lethbridge, AB T1K 3M4, Canada.

The phosphate-binding loop (P-loop) is a conserved sequence motif found in mononucleotide-binding proteins. Little is known about the structural dynamics of this region and its contribution to the observed nucleotide binding properties. Understanding the underlying design principles is of great interest for biomolecular engineering applications. We have used rapid-kinetics measurements *in vitro* and molecular dynamics (MD) simulations *in silico* to investigate the relationship between GTP-binding properties and P-loop structural dynamics in the universally conserved Elongation Factor (EF) Tu. Analysis of wild type EF-Tu and variants with substitutions at positions in or adjacent to the P-loop revealed a correlation between P-loop flexibility and the entropy of activation for GTP dissociation. The same variants demonstrate more backbone flexibility in two N-terminal amino acids of the P-loop during force-induced EF-Tu·GTP dissociation in Steered Molecular Dynamics simulations. Amino acids Gly18 and His19 are involved in stabilizing the P-loop backbone via interactions with the adjacent helix C. We propose that these P-loop/helix C interactions function as a conserved P-loop anchoring module and identify the presence of P-loop anchors within several GTPases and ATPases suggesting their evolutionary conservation.

The phosphate-binding loop (P-loop) is a conserved sequence motif found in the superfamily of P-loop nucleoside triphosphate hydrolases (P-loop NTPases)[1]. The P-loop, also known as the Walker A motif, has the consensus sequence GxxxxGK(S/T) and contributes to the binding of nucleotides[2,3]. Comparison of the X-ray structures of over 450 proteins from various functional backgrounds has revealed that, despite the low sequence conservation of the P-loop, the three-dimensional structure is retained among 13 different superfamilies of mononucleotide-binding proteins[4]. Thus, the P-loop appears to be a versatile evolutionary solution to mononucleotide binding with great potential for the rational design of nucleotide binding properties in bioengineering applications.

In spite of the well-conserved three-dimensional structure of the P-loop in the presence of nucleotides, several P-loop NTPases have been crystallized with 'alternative' P-loop conformations in their respective nucleotide-free forms. These include the ATPases adenylate kinase[5] and MutS[6] as well as the G-proteins Rac1[7], Ras[8], Elongation Factor (EF) G[9], Gs[10], and EF-Tu[11]. This indicates that, although highly conserved in structure when bound to a nucleotide, the structural dynamics of the P-loop may be a functionally relevant design feature available in P-loop NTPases. In this regard, the G-proteins Rac1, Ras, Gs, and EF-Tu are particularly interesting as in each of these structures the G-protein is bound to its respective Guanine nucleotide Exchange Factor (GEF), which stimulates nucleotide dissociation. Thus, conformational changes in the P-loop may be a common strategy contributing to GEF-stimulated nucleotide exchange in G-proteins. A detailed understanding of the design principles underlying the P-loop is of general interest for biomolecular engineering, and in particular for the rational design of molecular switches such as GTPases that require GDP/GTP exchange for their activation.

Ultimately, the relationship between P-loop conformational changes and nucleotide-binding properties requires an understanding of P-loop structural dynamics. Mounting evidence suggests that conformational changes or functions occurring on the microsecond to second timescale are slave to shorter-timescale fluctuations within proteins (picosecond to millisecond)[12–15]. This suggests that nanosecond-timescale molecular dynamics (MD) simulations can provide insight into protein dynamics occurring on the millisecond to seconds timescale. Therefore, MD simulations are valuable tools for studying and assessing structural dynamics as they can simulate motions within proteins at atomic resolution and provide critical information when carefully interpreted in the context of experimental data. Here we report an investigation of P-loop structural dynamics in EF-Tu using MD

simulations to provide atomic-resolution descriptions of P-loop motions. In conjunction, we present rapid-kinetics experiments that reveal the thermodynamic properties of EF-Tu·GTP interaction as well as the activation barrier for dissociation. Based on this we propose that the structural dynamics of the P-loop can be used to modulate nucleotide binding properties in EF-Tu and that this principle can likely be extended to a broader class of P-loop NTPases.

Results

In EF-Tu, two different P-loop conformations have been identified: one in the presence of a bound guanine nucleotide[16–18] and one in complex with the nucleotide exchange factor EF-Ts[11]. During the transition from the nucleotide-bound form of EF-Tu to the EF-Tu·EF-Ts complex, a flip of the peptide backbone between Valine 20 and Aspartate 21 occurs in EF-Tu's P-loop[11]. The rapid dissociation of nucleotides from EF-Tu·nucleotide·EF-Ts complexes[19] strongly implies a correlation between the P-loop conformation and the nucleotide binding properties as noted by others[11]. Similarly, the Histidine 118 to Alanine variant of EF-Tu, which lacks the Gly18···His118 hydrogen bond between the P-loop and helix C, was previously shown to bind nucleotides with a ten-fold reduced affinity when compared to wild type EF-Tu[20]. The authors suggested that removal of this hydrogen bond causes an increase in P-loop flexibility and in turn, lower nucleotide-binding affinities. Here we wanted to test the following hypotheses: (1) P-loop structural dynamics mediate GTP-binding properties in EF-Tu and (2) P-loop structural dynamics can be regulated by adjacent amino acids.

Based on the available EF-Tu structures, sequence conservation, and our own MD simulations (*vide infra*), we have identified two amino acid positions that are likely to be critical for the structural dynamics and overall flexibly of the P-loop in EF-Tu. Histidine 22 is located in the P-loop (Fig. 1), is 100% conserved among bacterial EF-Tus[21], and has previously been shown to form a transient hydrogen bond to the adjacent second shell residue Aspartate 109[22]. Although important for EF-Ts-modulated nucleotide exchange, this hydrogen bond is not important for fine-tuning nucleotide binding in the EF-Tu·GTP complex[22]. Interestingly, Histidine 22 is in close proximity to a highly (>99%) conserved Methionine in position 112 (Fig. 1). We therefore reasoned that by packing against Methionine in position 112 Histidine 22 might play a role in limiting the internal structural dynamics (flexibility) of the P-loop as well as restricting the mobility of the P-loop as a whole. To address this we have constructed a Histidine 22 substitution variant containing Glycine in this position (EF-Tu_{H22G}) to increase the internal flexibility and mobility of the P-loop. Also, we have introduced Glycine or Alanine in position 112 (EF-Tu_{M112G} and EF-Tu_{M112A} respectively) to increase the mobility of Histidine 22 and, in turn, the P-loop. We also constructed a Leucine variant (EF-Tu_{M112L}) to control for altering the space requirements of the side chain in position 112 without affecting the contacts between this position and the P-loop.

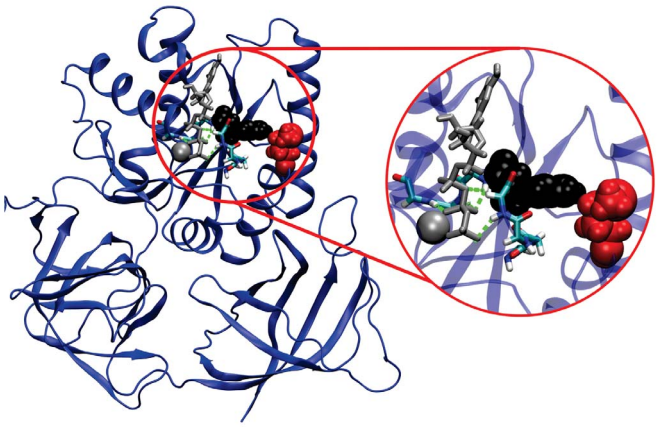

Figure 1 | His22 and Met112 form close contacts in the secondary shell surrounding the P-loop of EF-Tu. The model of *E. coli* EF-Tu·GTP is shown in cartoon representation after 10 ns of molecular dynamics simulation. Bound GTP and Mg^{2+} are shown as sticks and space-filling, respectively, both coloured silver. The backbone atoms of the P-loop are shown as sticks and hydrogen bonds between P-loop amide hydrogen atoms and phosphate oxygen atoms of GTP are shown as green dashed lines. His22 (black) of the P-loop and Met112 (red) of the adjacent coil are shown in space-filling representation.

Substitution of Histidine 22 with Glycine increases the entropy barrier for GTP dissociation. The GTP-binding properties of EF-Tu_{H22G} were investigated using the pre-steady state kinetics approach previously described by us[19,22]. The dissociation and association rate constants for EF-Tu_{H22G}·mant-GTP and EF-Tu_{wt}·mant-GTP (wild-type EF-Tu) were determined accordingly (Fig. 2a and b) and are summarized in Table 1. Surprisingly, for EF-Tu_{H22G} the rate constant for GTP dissociation (k_{off}) is approximately 3-fold smaller than for EF-Tu_{wt}. A similar difference was observed in the rate constant for mant-GTP association (k_{on}). This corresponds to an approximately 10-fold higher affinity of EF-Tu_{H22G} for mant-GTP compared to EF-Tu_{wt} (Table 1), inconsistent with the expectation that replacing the Histidine side chain in position 22 with a hydrogen would increase the internal flexibility of the P-loop and reduce the GTP-binding affinity of EF-Tu (*vide supra*).

To identify the reason for the observed difference between EF-Tu_{wt} and EF-Tu_{H22G}, we determined the activation entropy for EF-Tu·mant-GTP dissociation. To this end the rate constants of mant-GTP dissociation (k_{off}) from EF-Tu_{wt} and EF-Tu_{H22G} were measured at temperatures ranging from 4°C to 37°C (Fig. 2c) and subsequently used to construct Eyring plots, with $\ln(k_{off}/T)$ on the *y*-axis, and 1/T on the *x*-axis. As expected, these plots exhibited linear behavior for both EF-Tu_{wt} and EF-Tu_{H22G}. When fit with a linear equation the resulting slope is equivalent to $-\Delta H^{0\ddagger}/R$ and the corresponding *y*-intercept equals $\ln(k_B/h) + \Delta S^{0\ddagger}/R$. The obtained differences in activation entropy and enthalpy between wild type and mutant EF-Tu are summarized in Table 1. Interestingly, the entropy of activation is higher for mant-GTP dissociation from EF-Tu_{H22G} than for EF-Tu_{wt} ($T\Delta S^{0\ddagger}_{H22G} - T\Delta S^{0\ddagger}_{wt} = (18 \pm 4)$ kJ/mol at 20°C), consistent with more conformational sampling in EF-Tu_{H22G} during the GTP dissociation as initially expected. While the increased entropy contribution should lower the transition state barrier and in turn increase the rate of EF-Tu_{H22G}·mant-GTP dissociation, this effect is counteracted by an enthalpy contribution. The enthalpy barrier for mant-GTP dissociation from EF-Tu_{H22G} is (19 ± 4) kJ/mol higher compared to EF-Tu_{wt}. The overall difference in $\Delta G^{0\ddagger}$, calculated from the mant-GTP dissociation rates at 20°C, is 2.3 kJ/mol which is within the error of the entropy and enthalpy calculations reported here. It is tempting to interpret the difference in $T\Delta S^{0\ddagger}$ between EF-Tu_{wt} and EF-Tu_{H22G} in the context of expected changes in P-loop structural dynamics (flexibility). However, experimentally measured changes in entropy reflect changes to the whole molecular system and cannot be simply assigned to a small subset of atoms in the system. Furthermore, the source of the additional enthalpy contribution to transition state barrier is unclear.

Molecular dynamics simulations reveal an additional hydrogen bond between GTP and the P-loop of EF-Tu_{H22G}. In order to provide insight into where the measured differences in activation entropy and enthalpy for mant-GTP dissociation from EF-Tu_{wt} and EF-Tu_{H22G} might originate, all-atom MD simulations were performed. MD simulations (10 ns per molecular system) were carried out using *apo* and GTP bound models of EF-Tu_{wt} and EF-Tu_{H22G} in order to relate these simulations to the respective equilibrium binding constants (K_D's) for GTP which describes the free energy difference between EF-Tu·GTP and EF-Tu + GTP. In

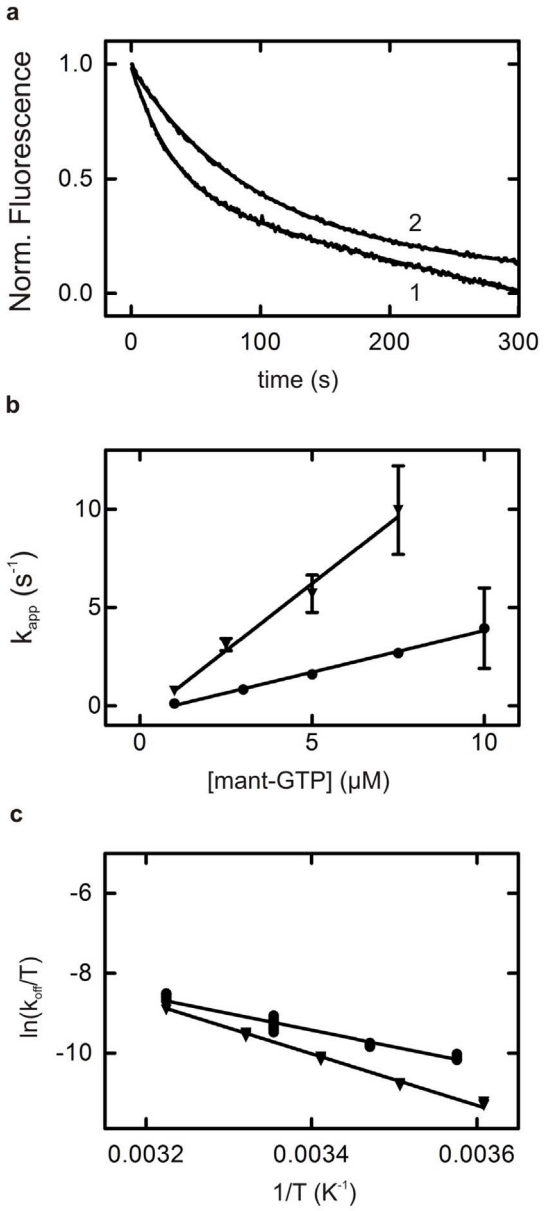

Figure 2 | Interaction of EF-Tu$_{H22G}$ and EF-Tu$_{wt}$ with mant-GTP. (a) Dissociation of mant-GTP was monitored upon mixing equal volumes of the EF-Tu·mant-GTP complex with unlabelled GTP to final concentrations of 0.15 μM and 25 μM, respectively. Single traces using (1) wild type EF-Tu and (2) EF-Tu$_{H22G}$ are shown along with the fitted exponential functions (smooth curves). (b) Mant-GTP association was monitored after mixing nucleotide free EF-Tu$_{wt}$ (•) or EF-Tu$_{H22G}$ (▼) (0.3 μM final concentration) with varying concentrations of mant-GTP. Data points represent the average of k_{app} values obtained from fits of individual traces and error bars represent the corresponding standard deviations. (c) Eyring plots of mant-GTP dissociation from EF-Tu$_{wt}$ and EF-Tu$_{H22G}$. Rate constants of mant-GTP dissociation (k_{off}) were determined at different temperatures. Data points represent rates obtained from fitting individual traces in replicate experiments; EF-Tu$_{wt}$ (•), EF-Tu$_{H22G}$ (▼).

addition, the transition state for GTP dissociation [EF-Tu···GTP]‡ is expected to possess some properties of EF-Tu·GTP and some of EF-Tu^{apo} [23]. Thus, analysis of these simulations can provide insight into the measured differences in $\Delta H^{0‡}$ and $T\Delta S^{0‡}$ for the dissociation of GTP from EF-Tu$_{wt}$ and EF-Tu$_{H22G}$. In the wild type simulation, interactions between EF-Tu and GTP are consistent with available X-ray crystal structures (Fig. 3) throughout the whole simulation. In particular Asparagine 135, Lysine 136, and Aspartate 138 of the NKxD motif maintain the guanine base-specific interactions, while the magnesium ion and the backbone amide nitrogen atoms of the four P-loop amino acids interact with the β- and γ-phosphates of GTP (Fig. 3a)[16]. In the MD simulations of EF-Tu$_{H22G}$·GTP, the same interactions are present. Remarkably, an additional hydrogen bond between the backbone amide bond of Glycine 22 and an oxygen atom of the β-phosphate is present in these simulations (Fig. 3b).

To assess the dynamics of the P-loop/GTP hydrogen bonds on a quantitative level, the N-H···O distances of each of the potential hydrogen bonds between the nucleotide phosphate and the P-loop were measured over the course of the simulations (Table S1). These distances were used to construct histograms, to which Gaussian functions were fit as previously described[22], (Fig. 3c and d). The obtained $N_{His22/Gly22}$-H···$O_{β1}$ distance distributions for EF-Tu$_{wt}$·GTP and EF-Tu$_{H22G}$·GTP were fit well by single Gaussian distributions centered over (3.1 ± 0.3) Å and (2.0 ± 0.2) Å, respectively. Thus, employing a conservative hydrogen bond criterion of 2.7 Å[22], indicates that an additional N_{His22}-H···$O_{β1}$ hydrogen bond occurs in the EF-Tu$_{H22G}$·GTP complex. This additional hydrogen bond between the P-loop and GTP in EF-Tu$_{H22G}$ will contribute to the observed higher binding affinity compared to EF-Tu$_{wt}$·GTP. More specifically, it would contribute to the measured increase in activation enthalpy for EF-Tu$_{H22G}$·GTP dissociation (*vide supra*) and is consistent with the slower GTP dissociation from EF-Tu$_{H22G}$ measured *in vitro* at 20°C.

Substitution of Histidine 22 with Glycine increases internal flexibility of the P-loop. Consistent with the measured increase in transition state entropy, substitution of Histidine 22 with Glycine likely increases the internal flexibility of the P-loop backbone at this position allowing the formation of an additional hydrogen bond to GTP (*vide supra*). In order to directly compare differences in backbone structural dynamics of EF-Tu, the backbone φ and ψ angles of every amino acid were measured over the course of our MD simulations. The resulting values were then used to construct a 'Ramachandran histogram' for each amino acid in each simulation, such that the conformational space explored by the backbone of each amino acid could be visualized (Fig. 4). Each Ramachandran histogram was then searched for distinct backbone conformations using a computer script described in Materials and Methods. The amino acids that occupied multiple conformations on the Ramachandran histogram were termed 'hot' amino acids, and represented in blue in Fig. 4b. These 'hot' amino acids are likely to contribute to the global entropy of EF-Tu, as entropy is proportional to the multiplicity of microstates in the system[24]. When comparing the occurrence of 'hot' amino acids between the nucleotide-bound and *apo* states of each variant we find that in the EF-Tu$_{H22G}$·GTP simulation Aspartate 21 is 'hot' while in EF-Tu$^{apo}_{H22G}$ Glycine 22 and Glycine 23 are 'hot'. In contrast, no amino acids interacting with GTP are hot in EF-Tu$_{wt}$ or the respective *apo* simulation. Our simulations therefore suggest that progression from EF-Tu·GTP to EF-Tu^{apo} causes a larger increase in P-loop backbone flexibility for EF-Tu$_{H22G}$ than for EF-Tu$_{wt}$, consistent with the larger $T\Delta S^{0‡}$ measured for EF-Tu$_{H22G}$·GTP dissociation. Furthermore, it demonstrates that higher P-loop backbone flexibility is correlated with measurably higher entropy of activation for EF-Tu·GTP dissociation. This suggests that internal flexibility of the P-loop does contribute significantly to EF-Tu·GTP dissociation kinetics and that the P-loop constitutes a structural element that can be used to fine-tune nucleotide-binding properties. In addition, the differences in P-loop structural dynamics identified using our Ramachandran histogram analysis (Fig. 4) provide a reasonable description of P-loop entropy.

Table 1 | Kinetic and thermodynamic parameters describing the interaction between EF-Tu and mant-GTP. Values for $\Delta\Delta H^{0\ddagger}$ and $\Delta\Delta S^{0\ddagger}$ were obtained from Eyring plots and represent the differences relative to wild type EF-Tu. Values for $T\cdot\Delta\Delta S^{0\ddagger}$ were computed at 20°C

EF-Tu	k_{off}/s^{-1}	$k_{on}/(10^5\ M^{-1}s^{-1})$	K_D/nM	$\Delta\Delta H^{0\ddagger}$/(kJ/mol)	$T\cdot\Delta\Delta S^{0\ddagger}$/(kJ/mol)
wt	0.030 ± 0.010	4.20 ± 0.20	70 ± 30	0	0
H22G	0.0116 ± 0.0004	13.7 ± 0.7	8.5 ± 0.5	19 ± 4	18 ± 4
M112G	0.0200 ± 0.0010	2.2 ± 0.1	91 ± 9	1 ± 5	2 ± 5
M112A	0.075 ± 0.003	1.0 ± 0.2	750 ± 180	0 ± 4	2 ± 4
M112L	0.150 ± 0.010	2.1 ± 0.2	700 ± 100	1.2 ± 2.4	6.1 ± 2.5

Amino acid 112 modulates GTP binding in EF-Tu in vitro. Based on its location relative to the P-loop (Fig. 1), the highly conserved Methionine 112 might be important for limiting the motions of the Histidine 22 side chain and subsequently P-loop mobility. We therefore constructed three EF-Tu variants (EF-Tu_{M112G}, EF-Tu_{M112A} and EF-Tu_{M112L}) and determined the rate constants (k_{on} and k_{off}) governing their interaction with GTP (Summarized in Table 1). Removal of the steric constrains imposed by the adjacent methionine in position 112 caused only a 2-fold decrease in the GTP association rate constant (k_{on}) and no significant effect on the corresponding dissociation rate constant (k_{off}) for EF-Tu_{M112G} (Table 1). This is consistent with a primary role of Histidine 22 in modulating the internal structural dynamics of the P-loop. Interestingly, when Methionine 112 is substituted with Alanine the affinity for GTP is reduced by approximately 10-fold (Table 1). This effect is even more pronounced in the Leucine substitution variant that exhibits an approximate 5-fold increased nucleotide dissociation rate constant and an approximately 2-fold decreased association rate constant. These effects on the association and dissociation rate constants clearly indicate that the amino acid in position 112 can modulate the nucleotide-binding properties in EF-Tu. In order to investigate the thermodynamic details of how the amino acid in position 112 modulates the GTP-binding properties in EF-Tu, we measured the temperature dependence of the mant-GTP dissociation rate constants for the three variants bearing substitutions in this position (Fig. S1). The obtained Eyring plots reveal that the $\Delta H^{0\ddagger}$ of mant-GTP dissociation for the three substitution variants are similar to wild type. This suggests that the observed effect is mainly entropic. Consistent with this observation, the EF-Tu_{M112L} variant shows a significant difference in $T\Delta S^{0\ddagger}$ when compared to EF-Tu_{wt} (6.1 ± 2.5 kJ/mol at 20°C) and in turn, accelerated nucleotide dissociation.

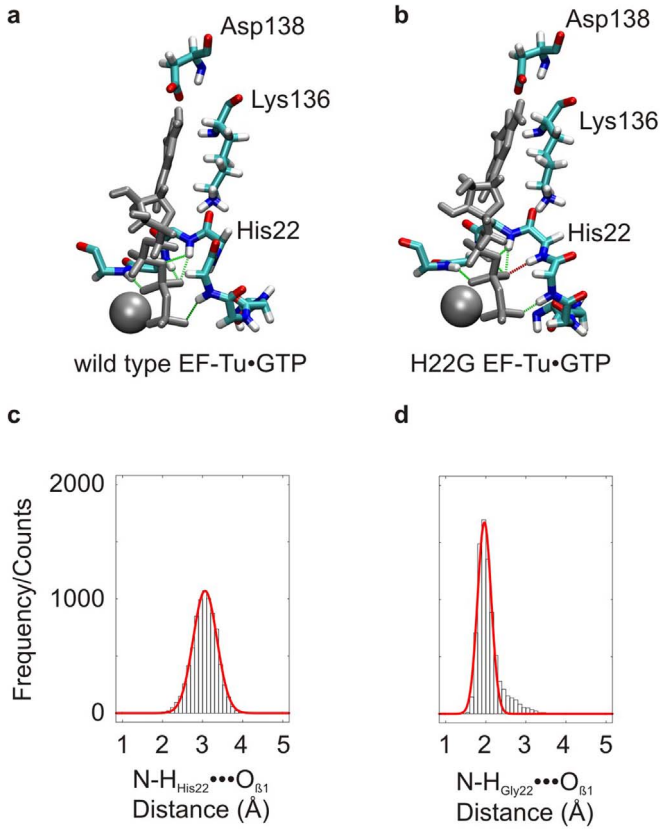

Figure 3 | The EF-Tu_{H22G} variant forms an additional hydrogen bond between the P-loop and bound GTP during molecular dynamics simulations. EF-Tu_{wt}·GTP (a) and EF-Tu_{H22G}·GTP (b) snapshots of the MD simulations were taken after 10 ns. Backbone atoms of the P-loop as well as Lysine 136 and Aspartate 138 of the NKxD motif are shown as sticks. GTP and the Mg^{2+} ion are shown as sticks and space-filling, respectively (silver). Hydrogen bonds identified between P-loop amino acids and GTP phosphates in both EF-Tu_{wt} and EF-Tu_{H22G} models are indicated by green dashed lines. The N-$H_{His22}\cdots O_{\beta1}$ hydrogen bond found in the EF-Tu_{H22G}·GTP model is shown as a red dashed line. The N-$H_{His22}\cdots O_{\beta1}$ distances were measured during MD simulation of EF-Tu_{wt}·GTP (c) and EF-Tu_{H22G}·GTP (d), and plotted in histograms. The solid red lines represent fits of the histograms to single Gaussian functions.

Substitution of Methionine 112 with Leucine weakens P-loop/helix C interactions and increases internal flexibility of the P-loop. To investigate the source of the increased entropy of activation for mant-GTP dissociation from EF-Tu_{M112L}, we have compared MD simulations of EF-Tu_{wt} and EF-Tu_{M112L}. Similar to EF-Tu_{H22G}, equilibrium simulations of the EF-Tu_{M112L}·GTP complex and EF-$Tu^{apo}{}_{M112L}$ were carried out, and amino acids occupying multiple backbone conformations were identified. However, no differences in the backbone flexibility of GTP-interacting amino acids were identified by this analysis. This suggests that the feature responsible for the increased entropic transition state barrier was not sampled in our "ground state" MD simulations. To overcome this apparent limitation, we performed steered molecular dynamics (SMD) simulations to evoke GTP dissociation *in silico* and explore the structural dynamics of the respective EF-Tu models outside the energy basins sampled during equilibrium MD simulations.

The SMD approach we applied introduces a spring with one end attached to the ligand and the other end attached to a point in space that moves at a constant velocity throughout the course of the simulation[25,26]. Five different 'pulling' directions (Fig. 5) as well as five different evenly spaced starting time points (6, 7, 8, 9, or 10 ns old equilibrium MD simulations) were investigated for each model in order to enable sampling of different dissociation pathways. In total, 25 different SMD simulations were performed for each model (EF-Tu_{wt}, EF-Tu_{H112G}, EF-Tu_{M112G}, EF-Tu_{M112A}, EF-Tu_{M112L}). Although the resulting trajectories do not necessarily represent the likely GTP-dissociation pathways, they enable perturbation of each molecular system out of its respective potential energy minimum. The backbone conformation of each amino acid was analyzed using 'Ramachandran histograms' similar to those in Fig. 4a, and the respective 'hot' amino acids were identified. The probability of each amino acid exploring different backbone conformations in a given

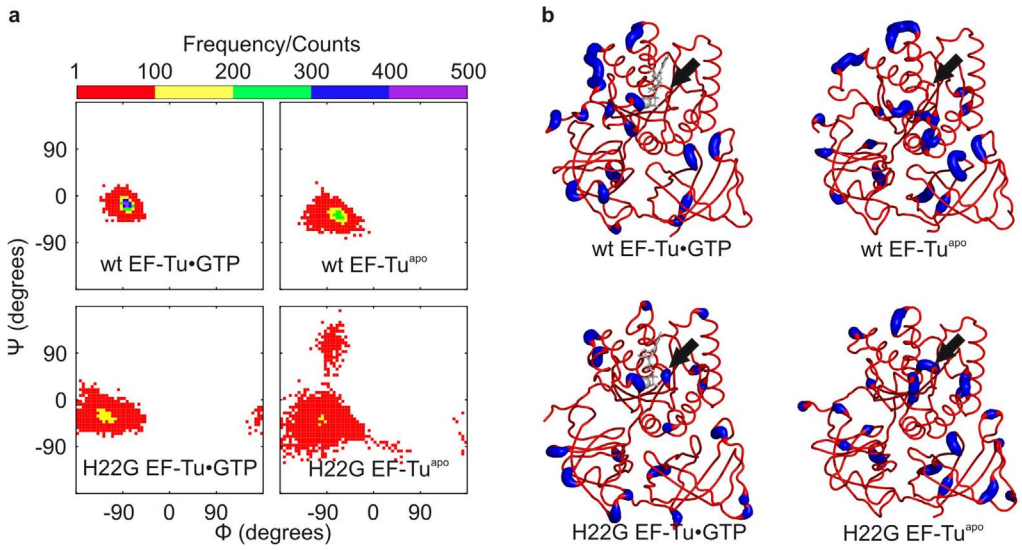

Figure 4 | The P-loop has higher entropy in MD simulations of EF-Tu$_{H22G}$ compared to EF-Tu$_{wt}$. (a) The backbone φ and ψ dihedral angles of amino acid 22 were measured during the 10 ns equilibrium MD simulations of EF-Tu·GTP, EF-Tu^{apo}, EF-Tu$_{H22G}$·GTP, and EF-Tu$^{apo}_{H22G}$, and plotted in histograms of φ vs. ψ. Each histogram is divided into bins with dimensions $\pi/32 \times \pi/32$. Each bin is coloured based on the occupancy according to the colour legend. Amino acids that occupied multiple conformations in histograms analogous to those in (a) were coloured blue on the structures presented in (b). Each structure presented in (b) is a snapshot taken after 10 ns of the respective MD simulation. The arrows in (b) indicate amino acid 22 in the P-loop.

SMD simulation was expressed as a percentage of the 25 total SMD simulations and represented as a colour on the respective EF-Tu·GTP model (Fig. 5). Based on this analysis it is evident that mainly the P-loop amino acids undergo additional backbone conformational changes during the SMD simulations and that their probability of being 'hot' is higher for EF-Tu$_{M112L}$ than for EF-Tu$_{wt}$ (Fig. 5, Table S2). This suggests that the P-loop of the EF-Tu$_{M112L}$ variant is indeed able to explore more conformations during GTP dissociation than that of the wild type, contributing to the increased entropy of activation and, in turn, a larger k_{off} for GTP dissociation.

Interestingly, comparing the P-loop amino acids reveals that the largest differences between EF-Tu$_{wt}$ and EF-Tu$_{M112L}$ are found in the two amino acids at the N-terminus of the P-loop: Glycine 18 and Histidine 19 (Fig. 5, Table S2). Neither of these amino acids explore alternative backbone conformations in SMD simulations of the wild type model, while both Glycine 18 and Histidine 19 explore multiple backbone conformations in 64% of SMD simulations for the EF-Tu$_{M112L}$ model. In order to better understand the structural basis of these differences, equilibrium MD simulations of EF-Tu$_{wt}$·GTP and EF-Tu$_{M112L}$·GTP were compared. In EF-Tu$_{wt}$·GTP, Glycine 18 and Histidine 19 are stabilized by hydrogen bonds to Histidine 118 and Glutamine 114, respectively (Fig. 6). However, in the simulations of EF-Tu$_{M112L}$·GTP, the His19···Gln114 hydrogen bond is not present while the Gly18···His118 hydrogen bond is only transiently stable (43.9%; Fig. 6a). This effect likely results from the slightly higher space requirements of the Leucine side chain compared to Methionine. In order to accommodate the branched Leucine side chain, the N-terminal tip of helix C is displaced approximately 3.6 Å away from the P-loop (Fig. 6b).

These results suggest that hydrogen bonds between His19/Gly18 of the P-loop and Gln114/His118 of helix C limit the structural dynamics of the P-loop providing a means of mediating the entropy of activation for EF-Tu·GTP dissociation.

Substituting Methionine 112 with Alanine does not increase P-loop dynamics. Interestingly, when comparing the P-loop dynamics of EF-Tu$_{M112A}$ (Table S2) it is most similar to EF-Tu$_{wt}$, which is consistent with the lack of a measureable difference in the entropy barrier for GTP dissociation. However, EF-Tu$_{M112A}$ has a ten-fold lower binding affinity (K_D) for GTP than EF-Tu$_{wt}$ (Table 1). The fact that the transition state energy barrier seems not to be affected by substituting Methionine 112 with Alanine, in conjunction with the 4-fold reduction in the association rate constant for EF-Tu$_{M112A}$

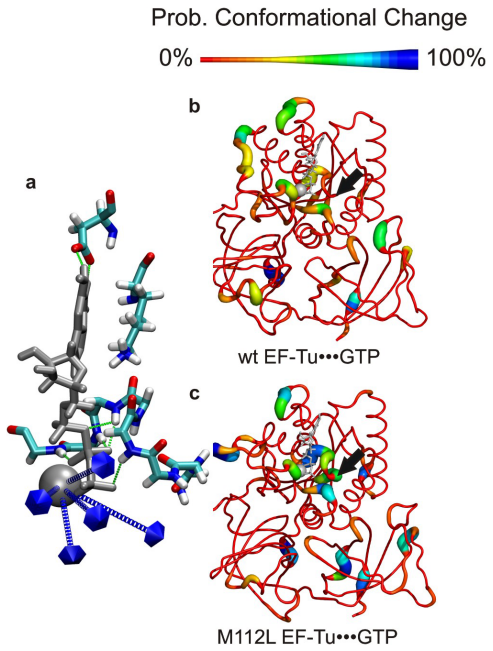

Figure 5 | The P-loop has higher entropy in steered MD simulations of EF-Tu$_{M112L}$ compared to EF-Tu$_{wt}$. (a) The five different directions used to pull GTP·Mg^{2+} out of the nucleotide binding pocket of EF-Tu are shown as blue arrows. The probability of a backbone conformational change during SMD simulation was computed in percent for each amino acid in EF-Tu$_{wt}$·GTP (b) and EF-Tu$_{M112L}$·GTP (c), and represented as a different colour and thickness on the corresponding structure. The structures in b and c are taken after 10 ns of the respective equilibrium MD simulation.

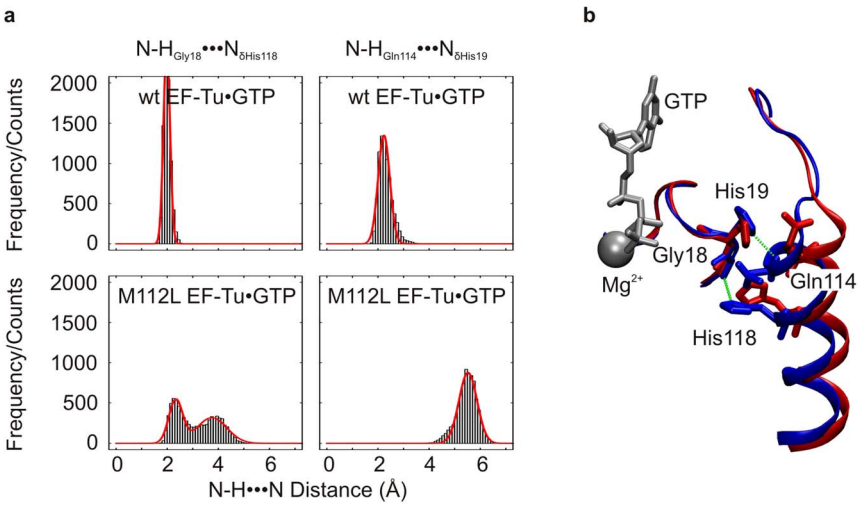

Figure 6 | Substitution of methionine 112 with leucine disrupts two P-loop/Helix C interactions in equilibrium MD simulations of EF-Tu·GTP. (a) Distances between N and H atoms of potential hydrogen bonds were measured during equilibrium MD simulations of EF-Tu$_{wt}$·GTP and EF-Tu$_{M112L}$·GTP. Distances were plotted as histograms and subsequently fitted to single- or double-Gaussian functions. (b) Comparison of EF-Tu$_{wt}$·GTP (blue) and EF-Tu$_{M112L}$·GTP (red) after 10 ns of equilibrium MD simulations reveals that displacement of Helix C is concomitant with disruption of Gly18···His118 and His19···Gln114 interactions. The P-loop and helix C from each protein are represented as cartoons, and pertinent sidechains are shown as sticks. The GTP molecule and Mg^{2+} from the wild type simulation are coloured silver and shown as sticks and space-filled representation, respectively. All hydrogen atoms are omitted for clarity, and green dashed lines represent N···N distances of the hydrogen bonds analyzed.

suggests a lower energy of the *apo* form of EF-Tu$_{M112A}$ compared to EF-Tu$_{wt}$ as the likely explanation. To this end we analyzed the equilibrium MD simulations of all EF-Tu simulations. Surprisingly, the *apo* form of the P-loop in EF-Tu$_{M112A}$ has a unique conformation compared to all other simulations, forming a single helical turn between amino acids 19 and 23 (Fig. S2). Additional energy will likely be required to disrupt the helical P-loop conformation in EF-Tu$^{apo}_{M112A}$ during GTP binding, consistent with the slower association rate constant (k_{on}) and ultimately with the larger experimentally determined equilibrium GTP binding constant (K_D) for EF-Tu$_{M112A}$.

Discussion

In contrast to our initial hypothesis, comparison of *in vitro* and *in silico* data from all EF-Tu variants investigated here suggests that an increase of internal flexibility in the P-loop does not necessarily alter nucleotide-binding properties in EF-Tu. For example, MD simulations of EF-Tu$_{M112G}$·GTP revealed two 'hot' amino acids in the P-loop (Aspartate 21 and Histidine 22) and a nucleotide affinity comparable to wild type EF-Tu (Table S3). However, in the EF-Tu$^{apo}_{M112G}$ simulation only Aspartate 21 is 'hot', indicating a net loss in hot amino acids progressing from EF-Tu$_{M112G}$·GTP to EF-Tu$^{apo}_{M112G}$. While one might expect a smaller activation entropy for EF-Tu$_{M112G}$·GTP dissociation compared to wild type, this change may be too small to be measured using the kinetic approach employed here. Substitution of Methionine in position 112 with Glycine therefore demonstrates that increased P-loop conformational flexibility does not necessarily result in accelerated nucleotide dissociation.

The comparison of P-loop flexibility simulated *in silico* and nucleotide-binding properties measured *in vitro*, reveals that backbone flexibility at positions 18 and 19, rather than other positions, correlate well with nucleotide-dissociation kinetics. Compared to EF-Tu$_{wt}$, variants EF-Tu$_{H22G}$ and EF-Tu$_{M112L}$ showed the largest changes in GTP-dissociation kinetics and were the only variants with significantly different activation entropies for GTP-dissociation. Interestingly, these variants were the only two in which Glycine 18 and Histidine 19 are 'hot' in 20% or more of the performed SMD simulations. The quantitative analysis of SMD results presented in Table S2 also support this hypothesis since Glycine 18 and Histidine 19 are more likely to explore multiple backbone conformations in SMD simulations of EF-Tu$_{H22G}$ and EF-Tu$_{M112L}$, than any other variant tested. This suggests that structural dynamics at positions 18 and 19 (in the P-loop) make a significant contribution to the entropy of nucleotide binding in EF-Tu.

For EF-Tu$_{M112L}$, increased backbone conformational freedom of Glycine 18 and Histidine 19 compared to wild type likely results from the disruption of His19···Gln114 and Gly18···His118 side chain··· backbone hydrogen bonds. Disruption of these stabilizing interactions between the P-loop and the adjacent helix C likely increases the entropy of the [EF-Tu···GTP]‡ transition state, lowering its free energy and accelerating nucleotide dissociation. This interpretation is consistent with the measured entropies of activation and rates of EF-Tu·mant-GTP dissociation (Table 1). A previous study of the EF-Tu$_{H118A}$ variant showed that upon elimination of the Gly18···His118 hydrogen bond between helix C and the P-loop, the rates of GTP and GDP dissociation were ten-fold faster than wild type[20]. This is in agreement with the data presented here and further supports our interpretation.

A functional requirement of the His19···Gln114 and Gly18··· His118 hydrogen bonds is supported by the finding that these amino acids are invariant in over 120 bacterial EF-Tu's[21], suggesting a functional conservation as a modulator module of P-loop structural dynamics within EF-Tu. In order to investigate if this modulator module is also present in other P-loop NTPases, we identified similar P-loop/helix C interaction modules in structures of six other G-proteins: EF-G (PDBID: 2BV3), FtsY (PDBID: 2Q9B), Ffh (PDBID: 2CO4), Ras (PDBID: 3L8Z), Rac1 (PDBID: 1MH1), and Ran (PDBID: 1MH1), as well as the two ATPases adenylate kinase (PDBID: 1AKE) and MutS (PDBID: 1E3M). Sequence alignments of the corresponding structural elements (Fig. S3), reveal that interactions between helix C and one or both of the two N-terminal P-loop amino acids are highly conserved in each of these P-loop NTPases. We therefore propose that the conserved P-loop/helix C interactions forms a 'P-loop anchor' that modulates P-loop entropy and, subsequently, nucleotide binding properties in P-loop NTPases.

P-loop anchors can employ hydrogen bonds as in EF-Tu, EF-G, Rac1, and Ran or hydrophobic interactions as in Ras, FtsY, Ffh,

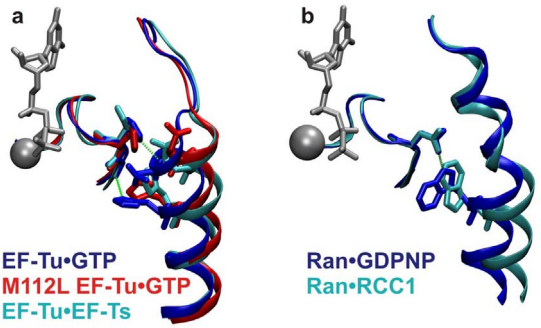

Figure 7 | Interactions between the P-loop and helix C are broken by guanine nucleotide exchange factors for EF-Tu and Ran. (a) Interactions between the P-loop and Helix C in EF-Tu_{wt}·GTP after 10 ns of MD simulation are compared to EF-Tu_{M112L}·GTP and the crystal structure of the EF-Tu·EF-Ts complex. (b) A similar interaction between the P-loop and adjacent helix of Ran compared in X-ray structures of Ran·GDPNP (PDBID: 1IBR) and Ran·RCC1(PDBID: 1I2M). The P-loops and helices are shown in cartoon representation; sidechain and/or backbone atoms of amino acids participating in hydrogen bonds are shown as sticks; GTP and Mg^{2+} are represented as sticks and space-filled representation, respectively. All hydrogen atoms are omitted for clarity, and green dashed lines connect heavy atoms involved in each hydrogen bond. All superimpositions were performed using P-loop backbone atoms.

adenylate kinase, and MutS. While the latter class appears weak in nature, it was previously identified as part of a conserved 'glycine brace' in some Ras family G-proteins[27], further supporting the P-loop anchor based modulator module as a conserved element in P-loop NTPases. The appearance of two different classes of P-loop anchors (hydrogen bond versus hydrophobic interactions) might, in fact, reflect differential modulation of P-loop structural dynamics.

Conformational changes in the P-loop of EF-Tu, induced by EF-Ts binding, have been proposed to stimulate EF-Tu·nucleotide dissociation[11]. Increased P-loop mobility would likely accelerate these conformational changes and, therefore, promote nucleotide dissociation. The observed peptide-flip between Valine 20 and Aspartate 21 in the P-loop of EF-Tu when bound to its exchange factor EF-Ts[11] complements the alternative P-loop conformations observed in our MD simulations (Fig. S2). The function of the P-loop anchor in modulating P-loop structural dynamics is supported by the observation that the P-loop anchor in EF-Tu is disrupted (Fig. 7a) in the crystal structure of the EF-Tu·EF-Ts complex[11]. This suggests that EF-Ts may have evolved to act on this conserved element to increase P-loop mobility during nucleotide dissociation. Similarly, X-ray crystal structures of Ran in complex with GDPNP or its GEF RCC1 reveal that GEF binding is concomitant with breaking the P-loop anchor (Fig. 7b) in this G-protein as well[28]. Interestingly, crystal structures of Ras and Rac1 bound to their respective GEFs demonstrate that disruption of the P-loop anchor interactions is not a requirement for GEF binding[7,29], but it seems likely that some GEFs have evolved in the context of this P-loop anchor in order to modulate P-loop structural dynamics and promote nucleotide dissociation.

We show that the structural dynamics of the P-loop can be used to modulate or fine-tune nucleotide binding properties in EF-Tu, and that this principle can likely be extended to a broader class of P-loop NTPases. From an engineering point of view, this provides a number of generalizable design principles. For example, the entropy contribution to the transition state barrier can be used to alter the nucleotide binding properties through manipulating the structural dynamics of the P-loop. This can be augmented with the stabilization of either the nucleotide-free and/or nucleotide-bound states of the P-loop, exploiting its ability to form additional interactions with the phosphates of the bound nucleotides as well as to fold into alternative conformations based on its inherent overall flexibility.

Our findings support the evolutionary conservation of a P-loop anchor that modulates the structural dynamics of the P-loop and fine-tunes nucleotide-binding properties.

Methods

Buffers and reagents. All stopped-flow experiments were performed in Buffer A (50 mM Tris-HCl pH 7.5, 70 mM NH_4Cl, 30 mM KCl, 7 mM $MgCl_2$). GTP was purchased from Sigma and 2′-/3′-O-N′-methylantraniloyl (mant)-GTP from JenaBioScience or Molecular Probes. DNA primers were purchased from Integrated DNA Technologies.

Mutagenesis. The plasmid pEECAHis[30], encoding for *E. coli* EF-Tu with a C-terminal hexahistidine tag, was used as the template for all mutagenesis reactions. The Quikchange™ method (Stratagene) employing two complementary primers was used in order to introduce the respective mutations. The primer sequences (only the coding stand primers are given) for construction of EF-Tu_{H22G}, EF-Tu_{M112L}, EF-Tu_{M112A} and EF-Tu_{M112G} variants were
(5′)GTACTATCGGCCACGTTGAC**GGT**GGTAAAACAACGCTG(3′),
(5′)ACGGCCCG**CTG**CCGCAGACTCGAGAGCACAT(3′),
(5′)TGACGGCCCG**GCG**CCGCAGACTCGAGAGCACATC(3′) and
(5′)TGACGGCCCG**GTG**CCGCAGACTCGAGAGCACATC(3′), respectively.
Template pDNA was degraded in a DpnI restriction digestion prior to transformation into competent *E. coli* NEB 5α cells (New England Biolabs) via heat shock. Single colonies were selected and isolated plasmid DNA was sequenced (MacroGen) to confirm the desired mutations.

Protein overexpression and purification. Each EF-Tu variant was overexpressed in *E. coli* BL21 (DE3) cells grown in liquid Luria-Bertani (LB) media containing 0.1 mg/mL ampicillin upon addition of isopropyl β-D-1-thiogalactopyranoside (IPTG) to a final concentration of 1 mM. Cells were opened by lysozyme treatment (1 mg/mL) in Buffer B (50 mM Tris-Cl pH 8.0 @ 4°C, 60 mM NH_4Cl, 7 mM $MgCl_2$, 7 mM β-mercaptoethanol, 1 mM phenylmethane-sulfonylfluoride, 50 μM GDP, 300 mM KCl, 10 mM imidazole, 15% glycerol) followed by sonication. Recombinant EF-Tu was purified as previously described[21] via affinity chromatography using Ni^{2+}-Sepharose resin (GE Healthcare) followed by size exclusion chromatography on a Superdex 75 column (GE Healthcare) in Buffer A. Purified EF-Tu was concentrated using a VivaSpin centrifugal concentration device (Sartorius; 30 kDa molecular weight cutoff), flash frozen in liquid nitrogen and stored at −80°C until use.

Rapid-kinetics measurements. EF-Tu·mant-GTP complexes for use in pre-steady state kinetics experiments were formed by incubation of 0.3 μM EF-Tu with 10-fold excess mant-GTP in the presence of 3 mM phosphoenolpyruvate and 10 μg/mL pyruvate kinase at 37°C for 30 minutes. Nucleotide-free EF-Tu was prepared by mixing EF-Tu with excess Buffer C (25 mM Tris-HCl pH 7.5 @ 37°C, 50 mM NH_4Cl, 10 mM EDTA) and subsequent incubation at 37°C for 30 minutes. EF-Tu was then separated from free nucleotide by size exclusion chromatography on a 10/300 Superdex 75 column (GE Healthcare) in Buffer D (25 mM Tris-Cl pH 7.5 @ room temperature, 50 mM NH_4Cl) prior to stopped-flow experiments. All solutions containing GTP or mant-GTP were incubated with phosphoenolpyruvate (3 mM) and pyruvate kinase (10 μg/mL) at 37°C for 30 minutes prior to use to convert any GDP or mant-GDP to the respective tri-phosphate form.

All stopped-flow experiments were carried out with a Kintek stopped-flow device (Model SF-2004). Fluorescence resonance energy transfer (FRET) from Tryptophan 184 in EF-Tu to the bound mant-GTP was monitored through a 400 nm long-pass cut-off filter (LG-4000-F: Newport Filters) upon excitation at 280 nm. Dissociation of mant-GTP was monitored as a decrease in mant fluorescence upon mixing equal volumes of EF-Tu·mant-GTP complex with unlabelled GTP to final concentrations of 0.15 μM EF-Tu, 1.5 μM mant-GTP, and 25 μM unlabelled GTP. The presence of excess unlabeled nucleotide in the reaction ensured that rebinding of mant-GTP was negligible. Thus, the system decays with the unimolecular rate constant k_{off}. The association of mant-GTP to EF-Tu was monitored upon mixing nucleotide-free EF-Tu (0.6 μM) with varying concentrations of mant-GTP (2–20 μM). The temperature was maintained constant during each experiment by circulating water (VWR model 1156D) through a water jacket surrounding the observation cell and syringes of the stopped-flow apparatus. Temperature was measured in the water jacket with a built-in electronic thermometer.

Data analysis. Single traces for all nucleotide dissociation experiments were fit using TableCurve software (Jandel Scientific), with single exponential equations as follows.

$$F = F_{\infty} + Ae^{-k_{app}\cdot t} + B\cdot t \quad (1)$$

Here F represents fluorescence, F_{∞} is the final fluorescence, A is the amplitude, k_{app} is the characteristic apparent rate constant, and B represents the linear time dependence of photobleaching. The average k_{app} value obtained from at least 4 fits yielded the respective dissociation rate constant k_{off}, and the error is represented by the corresponding standard deviation. For mant-GTP association experiments, individual traces were fit with the single exponential (Equation 2).

$$F = F_{\infty} + Ae^{-k_{app} \cdot t} \quad (2)$$

Under these pseudo-first order conditions, the apparent rate (k_{app}) of mant-GTP binding to EF-Tu is equal to k_{on}[mant-GTP] + k_{off}. The association rate constant k_{on} was determined by plotting the apparent rate of EF-Tu·mant-GTP formation as a function of the mant-GTP concentration followed by linear regression (Prism, GraphPad Software). The slope of this fit corresponds to the respective association rate constant (k_{on}). The temperature dependence of mant-GTP dissociation was analyzed by constructing Eyring plots: $\ln(k_{off}/T)$ as a function of inverse absolute temperature ($1/T$). Linear regression was performed to fit the data (Prism, GraphPad Software). The Eyring equation can be expressed as follows[31].

$$\ln\left(\frac{k_{off}}{T}\right) = \frac{-\Delta H^{0\ddagger}}{R}\left(\frac{1}{T}\right) + \frac{\Delta S^{0\ddagger}}{R} + \ln\left(\frac{k_B}{h}\right) \quad (3)$$

In Equation 3, R is the ideal gas constant (8.3145 J K^{-1} mol^{-1}), k_B is the Boltzman constant (1.3807×10^{-23} J K^{-1}), h is Planck's constant (6.6261×10^{-34} J s), $\Delta H^{0\ddagger}$ is the enthalpy of activation for mant-GTP dissociation, $\Delta S^{0\ddagger}$ is the entropy of activation for mant-GTP dissociation, and ^{0} indicates the molar standard state. The slope of the resulting fit is equal to $-\Delta H^{0\ddagger}/R$, and the y-intercept was $\ln(k_B/h) + \Delta S^{0\ddagger}/R$.

All-atom model construction. The all-atom model of *E. coli* EF-Tu·GTP was constructed and minimized as previously described[22]. In brief, a homology model of *E. coli* EF-Tu was constructed based on the X-ray crystal structure of *Thermus aquaticus* EF-Tu in complex with GDPNP (PDBID: 1EFT). To construct the EF-Tu·GTP model, the GDPNP and Mg^{2+} ligands from the crystal structure (PDBID: 1EFT) were included, and GDPNP was changed to GTP by hand. For the EF-Tu^{apo} model, nucleotide and Mg^{2+} ligands were omitted. Water molecules within 10 Å of the protein in the template structure were placed in the model. Additional water molecules were added using the Solvate package in VMD[32] to generate a box of TIP3 water molecules extending at least 10 Å from the protein in each direction. The solvated system was minimized in NAMD[25] and ionized using the Autoionize function in VMD[32] as described[22]. EF-Tu variants were constructed using the Mutator plugin in VMD[32] starting from the minimized *E. coli* EF-Tu·Mg^{2+}·GTP or EF-Tu^{apo} model.

Equilibrium molecular dynamics. All molecular dynamics calculations were performed using NAMD 2.6[25], the CHARM22 parameters for proteins[33], and CHARMM27 parameters for nucleic acids[34]. MD simulations were performed with a 0.5 fs step size in an NPT ensemble with the use of periodic boundary conditions. The pressure was maintained at one atmosphere using a Nosé-Hoover Langevin piston, and the temperature was controlled using Langevin dynamics. Non-bonded interactions were computed with a 12 Å cutoff and a 10 Å switching distance. Van der Waals and short-range electrostatic interactions were computed every 0.5 fs, and long-range electrostatics were computed every 1 fs. Each EF-Tu model was equilibrated at 300 K and 350 K for 150 ps in two independent simulations. After equilibration the model at 350 K was cooled to 300 K by applying the atomic velocities from the 300 K equilibration to the structure obtained from equilibration at 350 K. Production simulations were allowed to develop for at least 10 ns using velocity rescaling to stabilize the temperature at 300 K.

Steered molecular dynamics. Steered molecular dynamics (SMD) simulations were initiated using coordinates and velocities from equilibrium MD simulations after 6 ns, 7 ns, 8 ns, 9 ns, and 10 ns. The SMD driving force was attached to the magnesium ion and had a spring constant of 5 kcal/mol/Å^2. Removal of Mg^{2+} from the binding pocket has previously been shown, using rapid kinetics, to induce dissociation of the nucleotide[19]. The spring was pulled at a rate of 0.1 Å/ps, in five different directions. Direction A was defined as the vector from C6 to N3 of GTP, so chosen to minimize interference with the protein. Direction B was defined as the vector from C6 to C2 of GTP. Directions C, D, and E were defined by rotating direction B $\pi/2$, π, or $3\pi/4$ radians around an axis defined by direction A. Each SMD simulation was carried out for 0.5 ns.

Analysis of MD simulations. Snapshots of equilibrium MD simulations were saved every 0.5 ps and compiled using the software Carma[35] to remove water molecules as well as the motion of the protein center-of-mass. All metrics were measured using TCL scripts written in house, evoked in VMD. Ramachandran histogram plots were prepared and analyzed by running scripts in the software R[36]. Two-dimensional histograms with bin sizes of $\pi/32 \times \pi/32$ radians^2 were constructed using the backbone φ and ψ data from each simulation. These metrics were measured every 0.5 ps for equilibrium MD simulations and 0.1 ps for SMD simulations. Each histogram was searched for local maxima, defined as a bin or group of bins that is/are surrounded by 3 bins of decreasing occupancy in both the x- and y- directions. This definition allows for two local maxima to be as close as $\pi/8$ radians apart (centre to centre distance).

Potential hydrogen bonding distances were measured from the hydrogen atom of the hydrogen bond donor to the hydrogen bond acceptor. Distances were plotted as histograms for each simulation using a 0.1 Å bin size. Equation 4 or 5 was fit to each histogram corresponding to a one Gaussian or two Gaussian fit, respectively[37].

$$\text{counts} = Ae^{\frac{-(x-\bar{x}_a)}{2\sigma_a^2}} \quad (4)$$

$$\text{counts} = Ae^{\frac{-(x-\bar{x}_a)}{2\sigma_a^2}} + Be^{\frac{-(x-\bar{x}_b)}{2\sigma_b^2}} \quad (5)$$

Here A and B represent the peak heights of populations A and B, $\bar{x}_a$ and $\bar{x}_b$ are the average distances for populations A and B, and σ_a and σ_b are the standard deviations for populations A and B.

1. Wilson, D., Madera, M., Vogel, C., Chothia, C. & Gough, J. The SUPERFAMILY database in 2007: families and functions. *Nucleic Acids Res.* **35**, D308–D313 (2007).
2. Wittinghofer, A. & Vetter, I. R. Structure-function relationship of the G domain, a canonical switch motif. *Annu. Rev. Biochem.* **80**, 943–971 (2011).
3. Walker, J. E., Saraste, M., Runswick, M. J. & Gay, N. J. Distantly related sequences in the α- and β-subunits of ATP synthase myosin, kinases and other ATP-requiring enzymes and a common nucleotide binding fold. *EMBO J.* **1**, 945–951 (1982).
4. Kinoshita, K., Sadanami, K., Kidera, A. & Go, N. Structural motif of phosphate-binding site common to various protein superfamilies: all-against-all structural comparison of protein-mononucleotide complexes. *Protein Eng.* **12**, 11–14 (1999).
5. Müller, C. W., Schlauderer, G. J., Reinstein, J. & Schulz, G. E. Adenylate kinase motions during catalysis: an energetic counterweight balancing substrate binding. *Structure* **4**, 147–156 (1996).
6. Lamers, M. H. *et al.* The crystal structure of DNA mismatch repair protein MutS binding to a G·T mismatch. *Nature* **407**, 711–717 (2000).
7. Chhatriwala, M. K., Betts, L., Worthylake, D. K. & Sondek, J. The DH and PH domains of Trio coordinately engage Rho GTPases for their efficient activation. *J. Mol. Biol.* **368** (2007).
8. Boriack-Sjodin, P. A., Margarit, S. M., Bar-Sagi, D. & Kuriyan, J. The structural basis of the activation of Ras by SOS. *Nature* **394**, 337–343 (1998).
9. Ævarsson, A. *et al.* Three-dimensional structure of the ribosomal translocase: elongation factor G from *Thermus thermophilus*. *EMBO J.* **13**, 3669–3677 (1994).
10. Rasmussen, S. G. F. *et al.* Crystal structure of the β_2 adrenergic receptor-Gs protein complex. *Nature* **477**, 549–555 (2011).
11. Kawashima, T., Berthet-Colominas, C., Wulff, M., Cusack, S. & Leberman, R. The structure of the *Escherichia coli* EF-Tu·EF-Ts complex at 2.5 Å resolution. *Nature* **379**, 511–518 (1996).
12. Carroll, M. J. *et al.* Evidence for dynamics in proteins as a mechanism for ligand dissociation. *Nat. Chem. Biol.* **8**, 246–252 (2012).
13. Henzler-Wildman, K. A. *et al.* A hierarchy of timescales in protein dynamics is linked to enzyme catalysis. *Nature* **450**, 913–916 (2007).
14. Tzeng, S.-R. & Kalodimos, C. G. Protein activity regulation by conformational entropy. *Nature* **488**, 236–240 (2012).
15. Nagel, Z. D., Dong, M., Bahnson, B. J. & Klinman, J. P. Impaired protein conformational landscapes as revealed in anomalous Arrhenius prefactors. *P. Natl. Acad. Sci. USA* **108**, 10520–10525 (2011).
16. Kjeldgaard, M., Nissen, P., Thirup, S. & Nyborg, J. The crystal structure of elongation factor EF-Tu from *Thermus aquaticus* in the GTP conformation. *Structure* **1**, 35–50 (1993).
17. Song, H., Parsons, M. R., Rowsell, S., Leonard, G. & Phillips, S. E. V. Crystal structure of intact elongation factor EF-Tu from *Escherichia coli* in GDP conformation at 2.05 Å resolution. *J. Mol. Biol.* **285**, 1245–1256 (1999).
18. Schmeing, T. M. *et al.* The crystal structure of the ribosome bound to EF-Tu and aminoacyl-tRNA. *Science* **326**, 688–694 (2009).
19. Gromadski, K. B., Wieden, H.-J. & Rodnina, M. V. Kinetic mechanism of elongation factor Ts-catalyzed nucleotide exchange in elongation factor Tu. *Biochemistry* **41**, 162–169 (2002).
20. Dahl, L. D., Wieden, H.-J., Rodnina, M. V. & Knudsen, C. R. The importance of P-loop and domain movements in EF-Tu for guanine nucleotide exchange. *J. Biol. Chem.* **281**, 21139–21146 (2006).
21. DeLaurentiis, E. I., Mo, F. & Wieden, H.-J. Construction of a fully active Cys-less elongation factor Tu: Functional role of conserved cysteine 81. *BBA-Protein Proteom.* **1814**, 684–692 (2011).
22. Wieden, H.-J., Mercier, E., Gray, J., Steed, B. & Yawney, D. A combined molecular dynamics and rapid kinetics approach to identify conserved three-dimensional communication networks in elongation factor Tu. *Biophys. J.* **99**, 3735–3743 (2010).
23. Hammond, G. S. A correlation of reaction rates. *J Am. Chem. Soc.* **77**, 334–338 (1953).
24. Dill, K. A. & Bromberg, S. *Molecular Driving Forces: Statistical Thermodynamics in Chemistry and Biology* [81–103] (Garland Science, New York, 2003).
25. Phillips, J. C. *et al.* Scalable molecular dynamics with NAMD. *J. Comput. Chem.* **26**, 1781–1802 (2005).
26. Park, S. & Schulten, K. Calculating potentials of mean force from steered molecular dynamics simulations. *J. Chem. Phys.* **120**, 5946–5961, doi:10.1063/1.1651473 (2004).

27. Neuwald, A. F. The glycine brace: a component of Rab, Rho, and Ran GTPases associated with hinge regions of guanine- and phosphate-binding loops. *BMC Struct. Biol.* **9** (2009).
28. Renault, L., Kuhlmann, J., Henkel, A. & Wittinghofer, A. Structural basis for guanine nucleotide exchange on Ran by the regulator of chromosome condensation (RCC1). *Cell* **105**, 245–255 (2001).
29. Margarit, S. M. *et al.* Structural evidence for feedback activation by Ras·GTP of the Ras-specific nucleotide exchange factor SOS. *Cell* **112**, 685–695 (2003).
30. Wieden, H.-J., Gromadski, K., Rodnin, D. & Rodnina, M. V. Mechanism of elongation factor (EF)-Ts-catalyzed nucleotide exchange in EF-Tu. Contribution of contacts at the guanine base. *J. Biol. Chem.* **277**, 6032–6036 (2002).
31. Tinoco, I., Sauer, K., Wang, J. C. & Puglisi, J. D. *Physical Chemistry, priciples and applications in biological sciences* [Challice, J. (ed)] [315–388] (Prentice Hall, Englewood Cliffs, NJ, 2002).
32. Humphrey, W., Dalke, A. & Schulten, K. VMD: visual molecular dynamics. *J. Mol. Graphics* **13**, 33–38 (1996).
33. MacKerell, A. D. *et al.* All-atom emperical potential for molecular modeling and dynamics studies of proteins. *J. Phys. Chem. B* **102**, 3586–3616 (1998).
34. Foloppe, N. & Mackerell, A. D. All-atom emperical force field for nucleic acids: I. Parameter optimization based on small molecule and condensed phase macromolecular target data. *J. Comput. Chem.* **21**, 86–104 (2000).
35. Glykos, N. M. Carma: A molecular dynamics analysis program. *J. Comput. Chem.* **27**, 1765–1768 (2006).
36. R: A Language and Environment for Statistical Computing (Vienna, Austria, 2012).
37. Brase, C. H. & Brase, C. P. *Understandable Statistics* [Schultz, L. (ed.)] [270–331] (Houghton Mifflin, Boston, 2003).

Acknowledgments

We thank Benjamin Nielson and Frédéric Gagnon for their help with cloning, site-directed mutagenesis and initial purification of proteins. This work was supported by funding from the Natural Sciences and Engineering Research Council of Canada (HJW: NSERC Discovery Grant; EM: NSERC Postgraduate Scholarships (PGS)), Alberta Innovates Technology Futures (HJW: New Investigator Award and iCORE Strategic Chair Program; EM Postgraduate Scholarships), the Canada Foundation for Innovation (CFI), and supercomputing resource allocations from WestGrid and Compute Canada.

Author contributions

H.J.W. and E.M. designed the research; E.M. and D.G. carried out all experiments; E.M. and H.J.W. wrote the manuscript. All authors reviewed the manuscript.

Additional information

Supplementary information accompanies this paper at http://www.nature.com/scientificreports

Competing financial interests: The authors declare no competing financial interests.

How to cite this article: Mercier, E., Girodat, D. & Wieden, H.-J. A conserved P-loop anchor limits the structural dynamics that mediate nucleotide dissociation in EF-Tu. *Sci. Rep.* **5**, 7677; DOI:10.1038/srep07677 (2015).